Nuclear energy density functionals grounded in *ab initio* calculations

F. Marino [1,2,*] C. Barbieri [1,2] A. Carbone,[3] G. Colò [1,2] A. Lovato [4,5] F. Pederiva,[6,5] X. Roca-Maza [1,2]
and E. Vigezzi [2]

[1]*Dipartimento di Fisica "Aldo Pontremoli," Università degli Studi di Milano, 20133 Milano, Italy*
[2]*Istituto Nazionale di Fisica Nucleare, Sezione di Milano, 20133 Milano, Italy*
[3]*Istituto Nazionale di Fisica Nucleare–CNAF, Viale Carlo Berti Pichat 6/2, 40127 Bologna, Italy*
[4]*Physics Division, Argonne National Laboratory, Argonne, Illinois 60439, USA*
[5]*Istituto Nazionale di Fisica Nucleare–Trento Institute of Fundamental Physics and Applications, 38123 Trento, Italy*
[6]*Dipartimento di Fisica, University of Trento, via Sommarive 14, 38123 Povo, Trento, Italy*

We discuss the construction of a nuclear energy density functional (EDF) from *ab initio* computations and advocate the need for a methodical approach that is free from *ad hoc* assumptions. The equations of state (EoSs) of symmetric nuclear and pure neutron matter are computed using the chiral NNLO$_{sat}$ and the phenomenological AV4$'$ + UIX$_c$ Hamiltonians as inputs to self-consistent Green's function (SCGF) and auxiliary field diffusion Monte Carlo (AFDMC) methods. We propose a convenient parametrization of the EoS as a function of the Fermi momentum and fit it on the SCGF and AFDMC calculations. We apply the *ab initio* based EDF to carry out an analysis of the binding energies and charge radii of different nuclei in the local density approximation. The NNLO$_{sat}$-based EDF produces encouraging results, whereas the AV4$'$ + UIX$_c$-based one is farther from experiment. Possible explanations of these different behaviors are suggested, and the importance of gradient and spin-orbit terms is analyzed. Our paper paves the way for a practical and systematic way to merge *ab initio* nuclear theory and density functional theory, while shedding light on some critical aspects of this procedure.

I. INTRODUCTION

The need to tackle the very complex nuclear many-body problem has inspired dramatic advances in the so-called *ab initio* methods in recent years [1–3]. These approaches aim at solving the many-nucleon Schrödinger equation in an exact or systematically improvable way by using a realistic model for the nuclear interaction in the vacuum. Examples of these approaches are the Green's function Monte Carlo (GFMC) and auxiliary field diffusion Monte Carlo (AFDMC) [4–6], self-consistent Green's function (SCGF) [7–10], coupled-cluster [2,11,12], in-medium similarity renormalization group [3,13], and many-body perturbation theory methods [14,15]. Successful nuclear structure calculations have been performed for low- and medium-mass nuclei [1,3,4,16], as well as in infinite nuclear matter [9,17,18] and neutron stars [19,20]. Although *ab initio* theory can now approach masses of $A \approx 140$ [21], its predictive power is affected by the large computational cost and full-scale studies of heavy nuclei are still out of reach.

In the heavy-mass region of the nuclear chart, the method of choice is density functional theory (DFT). Originally introduced in condensed matter, DFT is a hugely popular method that finds application in several areas of physics, ranging from quantum chemistry [22–25] to nuclear physics [26–31]. In the latter case, it represents the only approach that allows one to cover almost the whole nuclear chart [26,27,30], with the partial exception of very light nuclei, and to study both ground states (g.s.) and, in its time-dependent formulation, excited states [29]. In principle, DFT provides an exact formulation of the many-body problem based on the Hohenberg-Kohn theorems [22,30,32], which state that all observables, starting from the total energy, can be expressed in a unique way as a functional of the one-body density (including spin densities and other generalized densities [33]). However, these theorems give no hints about the actual form of such functional, which is dubbed as the energy density functional (EDF). Hence, in practice, DFT turns out to be an approximate, albeit very powerful, method. In particular, most relativistic [34] and nonrelativistic [26–28] nuclear EDFs are designed in an empirical manner. A reasonable ansatz for the functional form is chosen and its actual parameters are fitted on experimental observables such as radii and masses of finite nuclei, or pseudo-observables such as the saturation density of symmetric nuclear matter [27,35]. The available EDFs are overall successful [26,30], e.g., the experimental binding energies are reproduced on average within 1–2 MeV and charge radii within 0.01–0.02 fm. However, it is unclear how to further improve the performance of traditional EDFs [36]. Despite attempts to frame DFT as an effective field theory (EFT), we still lack guiding principles for the systematic improvement of nuclear EDFs [37]. Existing EDFs are affected by uncontrolled extrapolation errors when applied to systems for

*francesco.marino@unimi.it

which scarce data are available, like neutron-rich nuclei or superheavy nuclei [26,38]. To solve these issues, a rethinking of the strategy to build the EDFs is in order.

It has already been recognized that surpassing the current limitations of nuclear EDFs requires a combination of the DFT and *ab initio* approaches [37,39,40]. Other attempts made in this direction include the density matrix expansion [41,42] and the use of *ab initio* calculations to constrain specific terms of the EDFs, while retaining a large amount of phenomenology [43–48].

In this paper, we advocate the need for pursuing a novel and more systematic strategy to ground nuclear DFT in *ab initio*. Our proposal is motivated by the existence of a well-established methodology in electronic DFT, known as the "reductionist" or nonempirical research program [25,49–51]. It aims at constructing a so-called Jacob's ladder [49] of increasingly more sophisticated EDFs, where one relies as much as possible on exact properties and *ab initio* calculations, and as little as possible on fits to the empirical data. The first rung of this ladder is the local density approximation (LDA), where an EDF that depends on the number densities alone is derived from the equations of state (EoSs) of uniform matter, i.e., the homogeneous electron gas (HEG) in the electronic case [22,23] and symmetric nuclear matter (SNM) plus pure neutron matter (PNM) in the nuclear case (we note that this has been, to a large extent, the spirit behind the works of Refs. [43,44]). The second rung introduces surface terms within the so-called gradient approximation (GA), constrained by *ab initio* simulations of nonuniform systems and by general principles when possible.

Nuclear physics poses additional challenges, however. In fact, the success of electronic DFT stems from the fact that the Coulomb force is known, and the dominant contribution to the total energy is the simple Hartree term [22]. On the other hand, the nuclear interaction has a rather complicated operator structure and is not uniquely determined [52], which allows for different predictions of some quantities and possibly leads to different equivalent EDFs. Moreover, the nuclear matter EoS is still not firmly established at variance with the HEG case [53]. Therefore, a truly systematic approach should take into account the nonuniqueness of the nuclear Hamiltonian, as well as to explore different many-body methods, to quantify the quality of predictions. An important final aspect is that the reductionist approach just outlined can be understood as a model selection procedure typical of machine learning applications [54,55]. Thus, Bayesian inference [56,57], and even more sophisticated learning tools, can be exploited to validate our EDFs and provide reliable uncertainties for their predictions

In this paper, we start the implementation of this program by carrying out a study of the LDA step for two distinct nuclear interactions. First, we make use of the simplified phenomenological AV4' + UIX$_c$ potential [58,59] in AFDMC calculations. Although this is the least sophisticated among the Argonne family [60], it is known to combine a reasonable accuracy in the description of finite nuclei [58] with a relatively modest computational effort. This allows for accurate AFDMC computations of isotopes as large as ^{90}Zr, as well as of both SNM and PNM. Moreover, within the scope of this

paper, this Hamiltonian is unique in that it allows one to test how our EDF construction method performs in the unfavorable case of hard interactions. Second, we use the established and accurate chiral interaction NNLO$_{sat}$ from Ref. [61] as input for SCGF computations [16,18]. We argue that the SNM and PNM EoSs are well parametrized in powers of the Fermi momentum k_F and perform a model selection procedure based on this ansatz. The resulting parametrizations of the EoS are used to construct the LDA EDFs, which are employed for g.s. calculations of closed-subshell nuclei and compared directly to the *ab initio* results for the same Hamiltonian that generated the EDF itself, as well as to the experiment. Lastly, a very preliminary exploration of the GA level is also discussed, although a full *ab initio* based study will be the subject of future works.

This paper is structured as follows. Section II provides an introduction to *ab initio* theory, presenting Hamiltonians (Sec. II A) and many-body methods (SCGF in Sec. II B, AFDMC in II C). Section III is devoted to the construction of the nuclear EDFs. The general framework is outlined in Sec. III A. The parametrization of the *ab initio* EoS is examined in Sec. III B. Then, LDA EDFs and GA EDFs are discussed in Sec. III C. In Sec. IV, the results are presented. The *ab initio* EoSs determined with NNLO$_{sat}$ and AV4' + UIX$_c$ are shown and interpolated (Sec. IV A). The corresponding LDA EDFs and GA EDFs are applied to finite nuclei in Secs. IV B and IV C, respectively. Lastly, concluding remarks are presented in Sec. V.

II. *AB INITIO*

A. Nuclear interactions

An effective description of nuclear systems at low energies can assume the nucleons as degrees of freedom and model their interactions through a nonrelativistic Hamiltonian, which includes two-nucleon (NN) and three-nucleon (3N) (and possibly many-nucleon) potential terms:

$$H = T + \sum_{i<j} V_{ij}^{NN} + \sum_{i<j<k} V_{ijk}^{3N} + \dots. \quad (1)$$

Determining the nuclear interaction is still a partially open problem, but realistic models of the nuclear force, that are fitted to reproduce accurately two- or few-body observables, e.g., NN scattering phase shift or the binding energy of the deuteron, do exist. Interactions are constructed in a phenomenological way [4,60], or by making use of chiral EFTs [52,62–64]. Chiral forces are derived in an order-by-order, low-momentum expansion consistent with the QCD symmetries. They are defined in momentum space, although coordinate-space versions of the so-called local forces have been put forward [65–69]. Since they are naturally cut off at high momenta by regulators [70], they elude the problem of handling the hard core, i.e., the strongly repulsive short-range behavior of the phenomenological potentials [10]. The calculations performed in this paper make use of the chiral NNLO$_{sat}$ and the phenomenological AV4' + UIX$_c$ interactions.

NNLO$_\text{sat}$ [61] is a chiral force that has been found to give a good simultaneous reproduction of binding energies and radii, as well as densities [21], up to medium-mass nuclei, while it also predicts a saturation point close to the empirical region. In spite of some drawbacks, e.g., the symmetry energy around and above saturation is underestimated [18], NNLO$_\text{sat}$ is still among the best performing and most used chiral Hamiltonians (see, e.g., Refs. [16,71]).

Argonne interactions are widely employed phenomenological potentials [4,59,60]. The most sophisticated of them is the Argonne v_{18} (AV18) NN force, which contains 18 spin/isospin operators. Simplified versions, more amenable to many-body calculations, have been devised [59]. Denoted as AVN′, these interactions contain a subset of N operators and are refitted in order to reproduce as many two-nucleon properties as possible. Together with the NN interaction, a three-nucleon force has to be introduced to reproduce the spectrum of light nuclei and saturation properties of infinite nucleonic matter [72]. In Refs. [58,73] it was found that the simple AV4′, which comprises only four operators,

$$O_{ij}^{p=1,...,4} = [1, \sigma_i \cdot \sigma_j] \otimes [1, \tau_i \cdot \tau_j], \quad (2)$$

complemented with the central term of the Urbana IX 3N interaction (UIX$_c$), yields reasonable ground-state energies of light and medium-mass nuclei—the binding energies deviate by about 10% from experiment. AV4′ + UIX$_c$ is therefore interesting for this exploratory paper, since it allows one to carry out accurate Monte Carlo studies of nuclear matter (both PNM and SNM) and of nuclei as large as ^{90}Zr. Moreover, the fact that AV4′ does not contain tensor or spin-orbit operators greatly simplifies the solution of the many-body problem with the AFDMC method.

B. SCGF

The SCGF method [7–10] provides a nonperturbative and systematically improvable solution to the Schrödinger equation for a system of A interacting fermions that is rooted on the concept of many-body propagators, also known as Green's functions. The central quantity is the one-particle propagator

$$g_{\alpha\beta}(\omega) = -\frac{i}{\hbar} \int dt \, e^{i\omega t} \langle \Psi_0 | T[c_\alpha(t) c_\beta^\dagger(0)] | \Psi_0 \rangle, \quad (3)$$

where greek letters label the states of a complete orthonormal single-particle basis, $c_\alpha(t)$ [$c_\alpha^\dagger(t)$] are the annihilation (creation) operators of a particle in state α at time t, and $T[\ldots]$ is the time ordering operator. The propagator $g_{\alpha\beta}(\omega)$ provides access to all one-body observables and to the ground-state energy; moreover, it gives information on the neighboring $A \pm 1$ nuclei, for example by providing the one-nucleon addition and removal energies [16]. The interest in SCGF lies in the wealth of information that can be accessed in a single stage, as well as in its computational cost scaling polynomially with the number of particles [8]. It is nonetheless a demanding method and fully converged results for g.s. energies are presently possible for mass numbers up to $A \approx 60$–90, depending on the chosen Hamiltonian, and for nuclear matter [10]. In a recent work [21], though, charge radii and charge density

distributions have been successfully obtained in a set of Sn and Xe isotopes up to $A = 138$.

In SCGF, the dressed Green's function is determined by solving the Dyson equation,

$$g_{\alpha\beta}(\omega) = g_{\alpha\beta}^{(0)}(\omega) + \sum_{\gamma\delta} g_{\alpha\gamma}(\omega) \Sigma_{\gamma\delta}^*(\omega) g_{\delta\beta}(\omega), \quad (4)$$

or the equivalent Gor'kov equation when one deals with open shell nuclei [74]. In Eq. (4), $g_{\alpha\beta}^{(0)}(\omega)$ is an unperturbed propagator. The $\Sigma_{\alpha\beta}^*(\omega)$ is the irreducible self-energy which is suitably written in a form that does not depend on a choice of the reference state but only on $g_{\alpha\beta}(\omega)$ itself. The Dyson or Gor'kov equations are in principle exact but the self-energy, $\Sigma_{\alpha\beta}^*(\omega)$, must be truncated in practical applications by keeping selected series of Feynman diagrams, hence resumming infinite subsets. State-of-the-art computations in finite nuclei exploit the algebraic diagrammatic construction method at order n [ADC(n)] [8,10], which is based on enforcing the correct analytic properties of the self-energy. ADC(n) is systematically improvable, as the exact solution is approached in the limit of large n. State-of-the-art computations use the ADC(2) many-body truncation in the Gor'kov formalism and reach ADC(3) for Dyson SCGF [10].

Nuclear matter is studied within the finite-temperature formalism, making use of the ladder approximation to the self-energy [8,9,75]. A fully self-consistent solution for the dressed propagator is found within such approximation, from which the total energy per nucleon can be obtained exploiting the modified Galitskii-Migdal-Koltun sum rule [76]:

$$E = \frac{1}{2\pi} \sum_{\alpha\beta} \int_{-\infty}^{E_F} (T_{\alpha\beta} + \omega\delta_{\alpha\beta}) \text{Im} \, g_{\alpha\beta}(\omega) d\omega - \frac{1}{2} \langle W \rangle, \quad (5)$$

where $T_{\alpha\beta}$ represents the kinetic energy term and $\langle W \rangle$ is a correction due to the inclusion of three-body interactions. The zero temperature limit for nuclear matter calculations is then taken exploiting the Sommerfeld expansion at low temperatures, which provides a reliable extrapolation of results to $T = 0$ [77].

C. AFDMC

Diffusion Monte Carlo (DMC) [4,5,78] methods solve the many-body Schrödinger equation by using imaginary-time projection techniques to enhance the ground-state component $|\Psi_0\rangle$ of a starting trial wave function $|\Psi_T\rangle$:

$$|\Psi_0\rangle \propto \lim_{\tau \to +\infty} |\Psi(\tau)\rangle = \lim_{\tau \to +\infty} e^{-(H-E_T)\tau} |\Psi_T\rangle, \quad (6)$$

where τ is the imaginary time and E_T is an estimate of the ground-state energy.

The application of DMC to nuclear physics is complicated by the presence of spin and isospin operators in the Hamiltonian. The two variants of continuum DMC algorithms, the GFMC [4,6] and the AFDMC [6,69,79], differ in the way they deal with the spin/isospin degrees of freedom. The GFMC method uses all of the $2^A \binom{A}{Z}$ spin-isospin components of the wave function and can treat highly realistic phenomenological and chiral interactions [66–68,80], but it is currently limited to nuclei with up to $A = 12$ nucleons. On the other hand, within

the AFDMC, the spin-isospin degrees of freedom are described by single-particle spinors, the amplitudes of which are sampled using Monte Carlo techniques based on the Hubbard-Stratonovich transformation, reducing the computational cost from exponential to polynomial in A. However, some of the contributions characterizing fully realistic nuclear forces, such as isospin-dependent spin-orbit contributions, cannot be treated in this way, yet. Hence, the AFDMC is limited to somewhat simplified interactions, but it can be applied to compute larger nuclei and nuclear matter.

The starting point of AFDMC calculations is a trial wave function, which is commonly expressed as the product of a long-range component $|\Phi\rangle$ and of two- plus three-body correlations:

$$|\Psi_T\rangle = \prod_{i<j} f_{ij}^c \prod_{i<j<k} f_{ijk}^c |\Phi\rangle. \tag{7}$$

In the above equation, we assumed the correlations to be spin-isospin independent. This simplified ansatz, consistent with Refs. [58,81,82], is justified by the fact that the AV4′ + UIX$_c$ Hamiltonian does not contain tensor or spin-orbit terms.

In finite nuclei, $|\Phi\rangle$ is constructed by coupling different Slater determinants of single-particle orbitals in the $|nl\,jm_j\rangle$ basis so as to reproduce the total angular momentum, total isospin, and parity of the nuclear state of interest [6]. On the other hand, infinite nuclear matter is modeled by simulating a finite number of nucleons on which periodic-box boundary conditions are imposed [83]. In this case, the single-particle states are plane waves with quantized wave numbers:

$$\mathbf{k} = \frac{2\pi}{L}(n_x, n_y, n_z) \quad n_i = 0, \pm 1, \pm 2, \dots, \tag{8}$$

where L is the size of the box and the shell closure condition must be met in order to satisfy translational invariance. As a consequence, the number of nucleons in a box must be equal to the momentum space "magic numbers" (1, 7, 19, 27, 33, ...) times the number of spin/isospin states: 2 for PNM, 4 for SNM. The equations of state of nuclear matter discussed in Sec. IV A are computed with 66 neutrons (PNM) and 76 nucleons (SNM) in a periodic box.

The AFDMC method has no difficulty in dealing with "stiff" forces that can generate wave functions with high-momentum components. This is in contrast with remarkably successful many-body approaches that rely on a basis expansion [11,12,84,85], which need relatively "soft" forces to obtain converged calculations. However, like standard diffusion Monte Carlo algorithms, the AFDMC suffers from the fermion sign problem, which results in large statistical errors that grow exponentially with τ. To control it, we employ the constrained-path approximation, as described in Refs. [6,69,86]. This scheme is believed to be accurate for Hamiltonians that do not include tensor or spin-orbit operators, as is the case for the AV4′ + UIX$_c$ potential. Expectation values of operators $\hat{O}$ that do not commute with the Hamiltonian are evaluated by means of the mixed estimator [4]

$$\langle \hat{O}(\tau) \rangle \approx 2 \frac{\langle \Psi_T | \hat{O} | \Psi(\tau) \rangle}{\langle \Psi_T | \Psi(\tau) \rangle} - \frac{\langle \Psi_T | \hat{O} | \Psi_T \rangle}{\langle \Psi_T | \Psi_T \rangle}. \tag{9}$$

Also, charge radii are estimated from the proton radii with the formula $r_{ch}^2 = r_p^2 + (0.8\,\mathrm{fm})^2$.

III. METHOD

A. Nuclear EDFs

The general structure of a nonrelativistic nuclear EDF is described in depth in Refs. [27,28,87]. In this section, the discussion is limited to even-even nuclei and to quasilocal EDFs, i.e., functionals that can be expressed as the volume integral of an energy density $\mathcal{E}(\mathbf{r})$ which is a function of the local densities [28] and their gradients. Nonlocal EDFs such as Gogny ones are not treated. Moreover, for simplicity pairing terms are neglected. Applications shall be limited to magic nuclei and to some closed-subshell ones.

Under these assumptions, the total energy is a functional of the time-even proton and neutron densities [number density $\rho_q(\mathbf{r})$, kinetic density $\tau_q(\mathbf{r})$, and spin-orbit density $\mathbf{J}_q(\mathbf{r})$, with $q = n, p$ [28,35] and reads

$$E = \int d\mathbf{r}\, \mathcal{E}(\mathbf{r}) = E_{\mathrm{kin}} + E_{\mathrm{pot}} + E_{\mathrm{Coul}}. \tag{10}$$

The kinetic energy term is given by [35]

$$E_{\mathrm{kin}} = \int d\mathbf{r}\, \mathcal{E}_{\mathrm{kin}}(\mathbf{r}) = \int d\mathbf{r}\, \frac{\hbar^2}{2m}\tau_0(\mathbf{r}). \tag{11}$$

The Coulomb contribution E_{Coul} is treated in the standard local Slater approximation [88]. The most general form of the potential term

$$E_{\mathrm{pot}} = \int d\mathbf{r}\, \mathcal{E}_{\mathrm{pot}}(\mathbf{r}) \tag{12}$$

is reported in Eqs. (48) and (49) of Ref. [28], and will be outlined in the next section. Neutron and proton densities have been recoupled into the isoscalar ($t = 0$) and isovector ($t = 1$) channels: isoscalar densities are total densities (e.g., $\rho_0 = \rho_n + \rho_p$), while isovector densities account for proton-neutron differences ($\rho_1 = \rho_n - \rho_p$). The coefficients of the various terms are all, in principle, functions of the density, although in practice most of them are set to a constant value [27]. The mean field equations are then derived by relating the densities to the single-particle orbitals $\phi_j(\mathbf{r})$ and applying the variational principle [87]:

$$\left[-\nabla \cdot \frac{\hbar^2}{2m_q^*(\mathbf{r})}\nabla + U_q(\mathbf{r}) + U_{\mathrm{Coul}}(\mathbf{r})\delta_{q,p} \right. \tag{13}$$

$$\left. + \mathbf{W}_q(\mathbf{r}) \cdot (-i)(\nabla \times \sigma) \right] \phi_j(\mathbf{r}) = \epsilon_j \phi_j(\mathbf{r}) \tag{14}$$

where

$$U_q = \frac{\delta E}{\delta \rho_q}, \quad \frac{\hbar^2}{2m_q^*(\mathbf{r})} = \frac{\delta E}{\delta \tau_q}, \quad \mathbf{W}_q = \frac{\delta E}{\delta \mathbf{J}_q}, \tag{15}$$

and $m_q^*(\mathbf{r})$, $U_q(\mathbf{r})$, and $\mathbf{W}_q(\mathbf{r})$ are called effective mass, mean field, and spin-orbit potential, respectively.

B. Parametrization of the *ab initio* EoS

Nuclear matter is an infinite and uniform system of nucleons interacting through the strong interaction only [20,89,90]. Nuclear matter is characterized by the nuclear EoS, which at zero temperature and for spin-unpolarized matter corresponds to the energy per nucleon $e = E/A$ as a function of the number densities of neutrons and protons, or of the total density ρ and the isospin asymmetry parameter $\beta = \frac{\rho_n - \rho_p}{\rho}$.

Uniformity implies that the orbitals are plane waves, leading to important simplifications of Eq. (10). In fact, the number and kinetic densities are uniform and related by [87]

$$\tau_q = \tfrac{3}{5}\rho_q k_{F,q}^2 = \tfrac{3}{5}(3\pi^2)^{2/3}\rho_q^{5/3}. \tag{16}$$

Moreover, the spin-orbit densities $\mathbf{J}_q$, as well as the derivatives of the density ($\nabla\rho_q = \Delta\rho_q = 0$), vanish. Thus only the ρ and $\rho\tau$ terms contribute to the nuclear matter energy, while the gradient ($\rho\Delta\rho$), spin-orbit ($\rho\nabla\cdot\mathbf{J}$), and tensor ($\mathbf{J}^2$) terms are nonvanishing in nonuniform systems only, such as nuclei, neutron drops, or semi-infinite matter.

These considerations suggest the following regrouping of the potential density $\mathcal{E}_{\text{pot}}$ for a generic nuclear system:

$$\mathcal{E}_{\text{pot}} = \mathcal{E}_{\text{bulk}} + \mathcal{E}_{\text{surf}}, \tag{17}$$

where

$$\mathcal{E}_{\text{bulk}} = \sum_{t=0,1} \left(C_t^\rho \rho_t^2 + C_t^\tau \rho_t \tau_t\right) \tag{18}$$

and

$$\mathcal{E}_{\text{surf}} = \sum_{t=0,1} \left(C_t^{\Delta\rho} \rho_t \Delta\rho_t + C_t^J \mathbf{J}_t^2 + C_t^{\nabla J} \rho_t \nabla\cdot\mathbf{J}_t\right). \tag{19}$$

These terms are called here bulk and surface contributions, respectively. Infinite matter probes only the bulk contributions, while surface terms are active in nonuniform systems.

The problem of determining the nuclear EoS is still partially unsettled [9,20,57,91], at stark variance with the case of the homogeneous electron gas in condensed matter, the EoS of which has been well known for decades from Monte Carlo calculations, as well as from analytical results in the low- and high-density limits [23]. By contrast, the choice of the nuclear Hamiltonian [14,17,18,72] and, to a lesser extent, of the many-body method [86] still impacts our knowledge of the theoretical nuclear EoS. Therefore, it is important to test our method on different EoSs, in order to better understand its potentialities and limitations.

Before using it as input to an EDF, the EoS must be parametrized. First of all, it is convenient to represent the energy per particle $e(\rho, \beta)$ as the sum of the kinetic energy per particle of the Fermi gas $t(\rho, \beta)$ and of a potential term $v(\rho, \beta)$ [47,89], consistently with the EDF structure (10):

$$e(\rho, \beta) = t(\rho, \beta) + v(\rho, \beta), \tag{20}$$

where

$$t(\rho, \beta) = \frac{t_{\text{sat}}}{2}[(1+\beta)^{\frac{5}{3}} + (1-\beta)^{\frac{5}{3}}]\left(\frac{\rho}{\rho_{\text{sat}}}\right)^{\frac{2}{3}}, \tag{21}$$

$$t_{\text{sat}} = \frac{3\hbar^2}{10m}\left(\frac{3\pi^2}{2}\right)^{\frac{2}{3}}, \quad \rho_{\text{sat}}^{\frac{2}{3}} \approx 22\,\text{MeV}, \tag{22}$$

and t_{sat} is the Fermi gas kinetic energy per particle of SNM at saturation density, $t_{\text{sat}} = t(\rho = \rho_{\text{sat}}, \beta = 0)$.

Next, an ansatz for the expression of the potential energy per particle $v(\rho, \beta)$ as a function of both ρ and β must be chosen. Presently, *ab initio* methods are mostly applied to PNM ($\beta = 1$) and SNM ($\beta = 0$). Hence, the dependence on β must be extrapolated from the limiting cases $\beta = 0$ and 1. Due to the isospin invariance of the nuclear force, odd powers of β vanish. Moreover, neglecting terms in β^4 is deemed accurate for densities close to saturation even for large asymmetries [90]. This quadratic dependence is adopted here too.

As far as the ρ dependence is concerned, one can reasonably expect that a limited number of powers of ρ should suffice for reproducing the theoretical EoS (see e.g., Refs. [17,89]). While a Taylor expansion in powers of the density is simple and useful [44,89], we argue that a better option is to postulate that the potential term be a polynomial of the Fermi momentum k_F, or equivalently of $\rho^{1/3}$ [47,48]. Heuristic motivations are the following: from a practical perspective, it grants a greater flexibility than a ρ expansion, to which it may eventually reduce as a special case. Also, it is known on an empirical basis that local EDFs need fractional powers of the density in order to get satisfactory predictions of the nuclear incompressibility [28,92], thus using k_F instead of ρ as an expansion variable is also in keeping with this latter necessity. Lastly, if the EoS is thought of as arising from a diagrammatic expansion, then powers of the Fermi momentum should appear naturally [47,93].

Combining the above assumptions, one can then write

$$v(\rho, \beta) = \sum_{\gamma=1/3...6/3} c_\gamma(\beta)\rho^\gamma = \sum_{\gamma=1/3...6/3} [c_{\gamma,0} + c_{\gamma,1}\beta^2]\rho^\gamma \tag{23}$$

where $c_{\gamma,0} \equiv c_\gamma(\beta = 0)$ and $c_{\gamma,1} \equiv c_\gamma(\beta = 1) - c_\gamma(\beta = 0)$. Up to this point, the model is still quite general. The only condition is that γ's have to be of the form integer/3. Now, we do not choose the potential *a priori* [47], but, in order to determine how many terms and which powers should enter the potential, we perform a model selection among all possible polynomials with at most six terms and γ not larger than 6 [Eq. (23)]. The following convention is employed: each model is identified by the exponents of the powers of k_F or $\rho^{\frac{1}{3}}$ it contains. For example, we refer to the polynomial $c_{\frac{2}{3}}\rho^{\frac{2}{3}} + c_{\frac{5}{3}}\rho^{\frac{5}{3}} + c_2\rho^2$ by (2,5,6). Each model is fitted on the SNM and PNM data points and the optimal parameters are determined by minimizing the mean squared error (MSE) [55,94]:

$$\sigma^2(c_{\gamma,0}, c_{\gamma,1}) = \frac{1}{N_{\text{data}}} \sum_{i=1}^{N_{\text{data}}} [e(\rho_i, \beta_i) - e_i]^2. \tag{24}$$

Cross-validation is used to evaluate the out-of-sample error [54,55], which we use to rank the different models. This is a more robust measure of goodness than the fit MSE or χ^2 [94]. The statistical analysis has been performed with the SCIKIT-LEARN library [95].

C. Construction of the EDFs

The simplest way to define an EDF based on the infinite matter EoS is LDA [23,31,44]. In LDA, one assumes that the same expression of the potential energy density valid in infinite matter holds for nonuniform densities $\rho_q(\mathbf{r})$ too. This approximation is well suited in particular for slowly varying density distributions, so that each small region of a generic (finite or infinite) system can be treated as a piece of bulk matter [23]. LDA provides the following expression for the bulk energy density $\mathcal{E}_{\text{bulk}}(\mathbf{r})$:

$$\mathcal{E}_{\text{bulk}}[\rho(\mathbf{r}), \beta(\mathbf{r})] = \rho(\mathbf{r})v[\rho(\mathbf{r}), \beta(\mathbf{r})]. \quad (25)$$

The LDA EDFs read

$$E_{\text{LDA}} = E_{\text{kin}} + E_{\text{bulk}} + E_{\text{Coul}} \quad (26)$$

and Eq. (13) simplifies, as $m^* = m$, $\mathbf{W}(\mathbf{r}) = 0$, and $U_q(\mathbf{r}) = U_q^{\text{bulk}}(\mathbf{r})$, where

$$
\begin{aligned}
U_q^{\text{bulk}}(\mathbf{r}) &= \frac{\delta E_{\text{bulk}}}{\delta \rho_q(\mathbf{r})} \\
&= \sum_\gamma \{(\gamma + 1)c_{\gamma,0} \\
&\quad + [(\gamma - 1)\beta(\mathbf{r}) + 2\tau_z]\beta(\mathbf{r}) c_{\gamma,1}\}\rho^\gamma(\mathbf{r}), \quad (27)
\end{aligned}
$$

for the potential term (23) and $\tau_z = +1$ for neutrons and $\tau_z = -1$ for protons. See Appendix A for the derivation.

While an *ab initio* based treatment of LDA is the main subject of this paper, it is known that such approximation is not sufficient to accurately describe nuclear systems [31]. Even for electronic DFT, where LDA is a solid starting point, it is understood that gradient terms are necessary for quantitatively accurate predictions [22]. In Sec. IV B, we will show that the LDA EDFs based on our chosen Hamiltonians give rather different outcomes. Hence, to better gauge the LDA, we also perform a preliminary analysis of a set of EDFs that include surface terms.

These functionals, that we name GA EDFs, are made by complementing LDA with isoscalar and isovector density-gradient terms and a one-parameter spin-orbit contribution. It must be understood that these GA EDFs are treated at a very preliminary level. For instance, $\rho\tau$ terms, that are known to be important in nuclear DFT and produce an effective mass $m^* \neq m$, are not discussed. Also, no rigorous statistical analysis is performed and no attempt to derive the surface terms from *ab initio* is made. These important themes are left for future studies.

Our GA EDFs have the following form:

$$E_{\text{GA}} = E_{\text{LDA}} + E_{\text{surf}} \quad (28)$$

where

$$E_{\text{surf}} = \int d\mathbf{r} \left[\sum_{t=0,1} C_t^\Delta \rho_t \Delta \rho_t \right.$$
$$\left. - \frac{W_0}{2} \left(\rho \nabla \cdot \mathbf{J} + \sum_q \rho_q \nabla \cdot \mathbf{J}_q \right) \right]. \quad (29)$$

Three parameters, C_0^Δ, C_1^Δ, and W_0, are introduced and are all assumed to be density-independent constants, as in widely used EDFs. The mean field equations (13) hold, with $m^* = m$ and $U(\mathbf{r}) = U_q^{\text{bulk}}(\mathbf{r}) + U_q^{\text{surf}}(\mathbf{r})$, where

$$\mathbf{W}_q(\mathbf{r}) = \frac{\delta E_{\text{surf}}}{\delta \mathbf{J}(\mathbf{r})} = \frac{W_0}{2}(\nabla \rho + \nabla \rho_q), \quad (30)$$

$$
\begin{aligned}
U_q^{\text{surf}}(\mathbf{r}) &= \frac{\delta E_{\text{surf}}}{\delta \rho_q} \\
&= 2C_0^\Delta \Delta \rho_0 + 2C_1^\Delta \Delta \rho_1 \tau_z - \frac{W_0}{2}(\nabla \cdot \mathbf{J} + \nabla \cdot \mathbf{J}_q)
\end{aligned}
$$
$$(31)$$

and U_q^{surf} is derived in Appendix B. Appendix C is dedicated to the concept of rearrangement energy of the EDF.

To tune the surface terms, a grid search on the three parameters C_0^Δ, C_1^Δ, and W_0 is carried out, although full-fledged fits will be necessary in later works. To benchmark the quality of the EDF predictions, the root mean square (rms) errors of the binding energies and the charge radii for the GA EDFs

$$\sigma_E\left(C_0^\Delta, C_1^\Delta, W_0\right) = \sqrt{\frac{\sum_{k=1}^{n_E} \left(E_k^{\text{th}} - E_k^{\text{exp}}\right)^2}{n_E}}, \quad (32a)$$

$$\sigma_{r_{\text{ch}}}\left(C_0^\Delta, C_1^\Delta, W_0\right) = \sqrt{\frac{\sum_{k=1}^{n_r} \left(r_k^{\text{th}} - r_k^{\text{exp}}\right)^2}{n_r}} \quad (32b)$$

are evaluated with respect to the experimental radii of ^{40}Ca, ^{48}Ca, ^{132}Sn, and ^{208}Pb and the binding energies of ^{40}Ca, ^{48}Ca, ^{90}Zr, ^{132}Sn, and ^{208}Pb [96]. All the DFT g.s. calculations are performed with the SKYRME_RPA code [88], which has been appropriately modified.

IV. RESULTS

A. Nuclear matter fits

The SNM and PNM equations of state employing the NNLO$_{\text{sat}}$ potential were computed in Ref. [18] using the SCGF method. The $T = 0$ limit is shown in Fig. 1 and explicit values are reported in Table I. In this paper, we consider simulations up to densities $\rho = 0.32$ fm^{-3}, as these are still compatible with the soft momentum cutoff of this interaction. The SNM EoS saturates at $\rho_{\text{sat}} = 0.15$ fm^{-3} and $E_{\text{sat}} = -14.7$ MeV. We performed fits on a set of points equally spaced by 0.01 fm^{-3} following the parametrizations discussed in Sec. III B. A fivefold cross-validation procedure was used to estimate the validation error and select the best model. The optimal choice was the polynomial (2,3,4,5,6), which achieves a very small MSE $= 10^{-8}$ MeV^2. This model is shown by the curves in Fig. 1 along with the complete *ab initio* dataset used in the fit.

The AV4$'$ + UIX$_c$ EoS has been calculated with the AFDMC method for several densities up to 0.40 fm^{-3}. To the best of our knowledge, this is the first application of AV4$'$ + UIX$_c$ to nuclear matter. The results are reported in Table II. The saturation point is located at an unusually high density ($\rho = 0.24$ fm^{-3}) and low energy ($E_{\text{sat}} = -23.7$ MeV) and the 3N contribution is instrumental in allowing the SNM EoS to
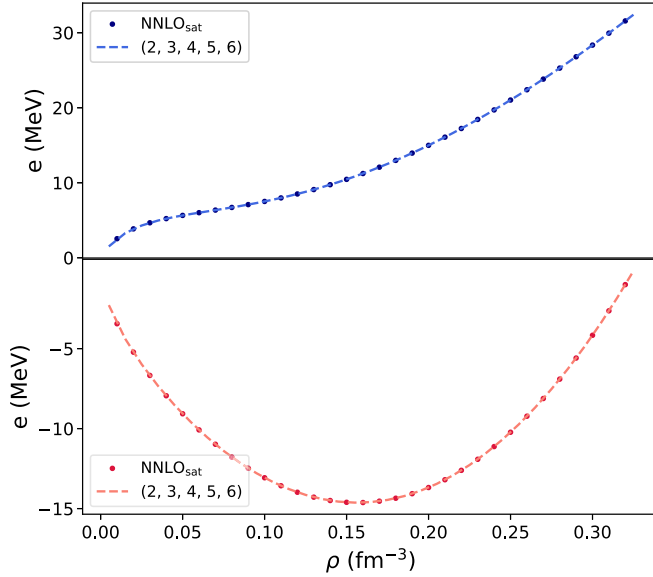
FIG. 1. Dots: SNM and PNM EoS computed with the NNLO$_{sat}$ interaction and the SCGF method. Dashed: model EoS (2,3,4,5,6) (see text).

saturate; in fact, AV4$'$ alone predicts no saturation before 0.50 fm^{-3} [97]. The smallest validation error (MSE = 0.06 MeV^2) is achieved by the (2,5,6) model, which is shown in Fig. 2 together with the *ab initio* EoS.

To sum up, parametrizing the nuclear EoS as a polynomial of the Fermi momentum has proved an effective ansatz. Two optimal models have been found, namely, (2,3,4,5,6) for the NNLO$_{sat}$ EoS and (2,5,6) for the AV4$'$ + UIX$_c$ EoS. The parameters of these models are reported in Table III.

B. Predictions of the LDA EDFs in finite nuclei

Two LDA EDFs are derived from the (2,3,4,5,6) and (2,5,6) parametrizations of the NNLO$_{sat}$- and the AV4$'$ + UIX$_c$-based EoS (Sec. IV A). These are then applied to closed-subshell nuclei and compared to experimental values, taken from Refs. [98,99], and to *ab initio* results. Full *ab initio* calculations are available for a set of nuclei up to ^{54}Ca for NNLO$_{sat}$

TABLE I. Energy per particle e computed with SCGF and the NNLO$_{sat}$ interaction at several densities ρ in both SNM and PNM.

ρ (fm^{-3})	e (MeV) SNM	e (MeV) PNM
0.04	-7.94	5.22
0.08	-11.78	6.71
0.12	-13.98	8.51
0.16	-14.62	11.23
0.20	-13.68	14.99
0.22	-12.61	17.24
0.24	-11.12	19.71
0.26	-9.22	22.40
0.28	-6.91	25.29
0.32	-1.00	31.58

TABLE II. Energy per particle e and standard errors (in parentheses) computed with AFDMC and the AV4$'$ + UIX$_c$ interaction at several densities ρ in both SNM and PNM.

ρ (fm^{-3})	e (MeV) SNM	e (MeV) PNM
0.04	-8.17 (1)	7.062 (5)
0.08	-13.60 (1)	11.075 (6)
0.12	-17.48 (1)	15.278 (8)
0.16	-20.74 (2)	20.20 (1)
0.20	-22.80 (1)	26.23 (1)
0.22	-23.42 (2)	29.66 (2)
0.24	-23.68 (3)	33.44 (3)
0.26	-23.58 (3)	37.47 (2)
0.28	-23.15 (3)	42.12 (3)
0.32	-21.10 (3)	52.26 (5)
0.36	-17.0 (1)	63.91 (6)
0.40	-12.21 (8)	77.51 (7)

and ^{90}Zr for AV4$'$ + UIX$_c$. Moreover, the NNLO$_{sat}$ densities for ^{90}Zr are available.

The discrepancy between theory and experiment for energies per nucleon (top) and charge radii (bottom) are shown in Fig. 3 for NNLO$_{sat}$ and the (2,3,4,5,6) EDF, as well as the GA-E and GA-r EDFs introduced later on (Sec. IV C). On the one hand, we can appreciate that NNLO$_{sat}$ predictions are very close to experiment. On the other hand, the LDA EDF, although less precise, exhibits interesting trends, since it enables one to reproduce heavier nuclei, especially from ^{90}Zr on, in a realistic way, with deviations smaller than 1 MeV/nucleon and 0.05 fm for the energies and radii, respectively. This is quite remarkable, as the LDA EDF incorporates only information on uniform matter. Also, it is unsurprising that light systems are less amenable to a local density treatment, since
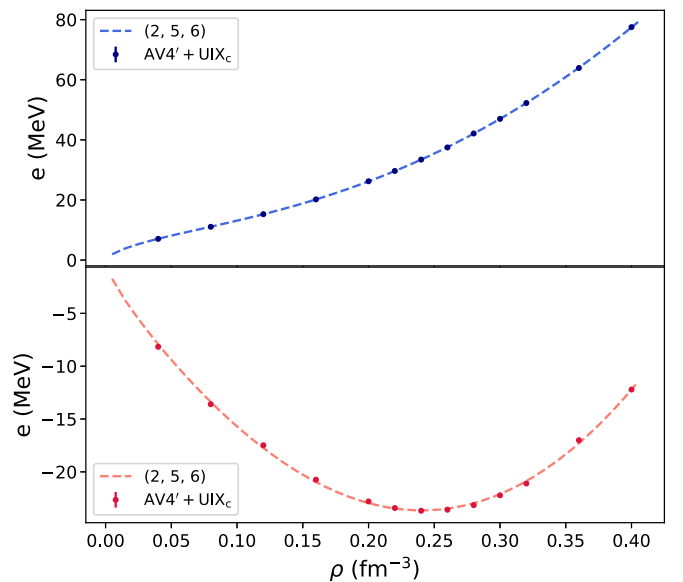

FIG. 2. Dots: SNM and PNM EoS computed with the AV4$'$ + UIX$_c$ interaction and the AFDMC method. The AFDMC statistical error bars are shown. Dashed: model EoS (2,5,6) (see text).

TABLE III. Coefficients of the optimal polynomial parametrizations (23) of the NNLO$_{sat}$ and AV4$'$ + UIX$_c$ EoS. The exponents γ and the corresponding parameters $c_{\gamma,0}$ and $c_{\gamma,1}$ are reported.

	γ	$c_{\gamma,0}$ (MeV fm$^{3\gamma}$)	$c_{\gamma,1}$ (MeV fm$^{3\gamma}$)
NNLO$_{sat}$	2/3	−182.41	16.93
	1	252.54	920.29
	4/3	−501.04	−4026.38
	5/3	63.80	6440.50
	2	669.42	−3646.52
AV4$'$ + UIX$_c$	2/3	−131.94	81.04
	5/3	−578.00	64.04
	2	901.30	48.97

surface effects are known to play a larger role for small values of A.

In Fig. 4, the deviation of the AV4$'$ + UIX$_c$, (2,5,6) EDF, and GA-E and GA-r EDF (Sec. IV C) predictions from experiment is shown. The outcome is puzzling, since, while the *ab initio* results are overall decent, the LDA EDF (2,5,6) strongly overbinds all the nuclei considered, by ≈ 10 MeV per nucleon. In addition, radii are underestimated with respect to both experiment and *ab initio*. Thus, in the case of the phenomenological interaction AV4$'$ + UIX$_c$, LDA alone has difficulties to capture the properties of the microscopic potential.

Number densities are then shown for the representative nuclei ^{48}Ca (Fig. 5) and ^{90}Zr (Fig. 6). In the NNLO$_{sat}$ case (top left), the (2,3,4,5,6) EDF density profile closely resembles the *ab initio* one, although it features slightly wider oscillation.
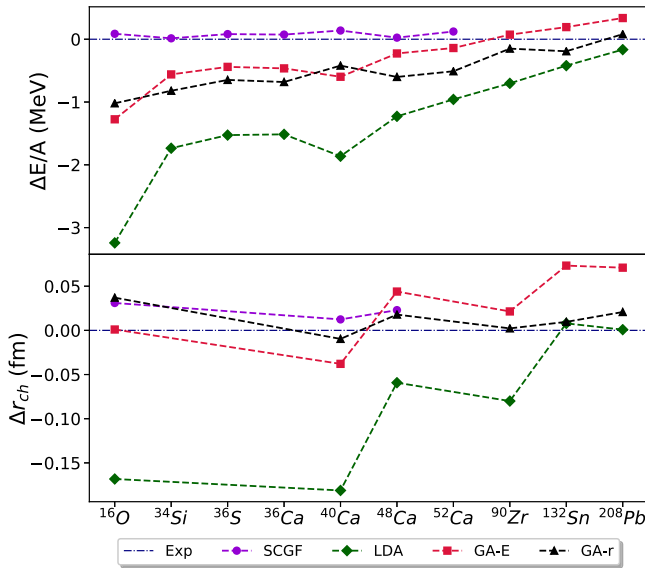

FIG. 3. Discrepancy between the predicted energies per nucleon (top) and charge radii (bottom) and the corresponding experimental values for a set of closed subshell nuclei. Results obtained with the NNLO$_{sat}$ interaction and with the LDA, GA-E, and GA-r EDFs are shown. The LDA EDF is derived from the (2,3,4,5,6) model EoS. The GA-E and GA-r EDFs are described in Sec. IV C.
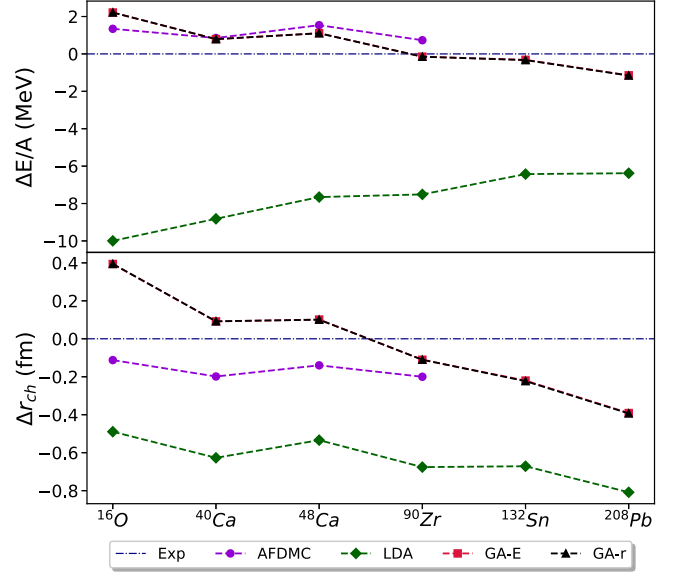

FIG. 4. Same as Fig. 3 (note the different scale), but for results obtained with the AV4$'$ + UIX$_c$ interaction and with the LDA, GA-E, and GA-r EDFs. The LDA EDF is based on the (2,5,6) EoS.

In the AV4$'$ + UIX$_c$ case (top right), instead, the (2,5,6) EDF and *ab initio* number densities differ considerably, as LDA produces definitely steeper density profiles, consistently with predicting sensibly smaller radii. Also, it somewhat overestimates the central density. In the bottom panel, the ^{48}Ca *ab initio* densities weighted by the squared radius, $r^2\rho(r)$, are compared. The r^2 factor emphasizes that AV4$'$ + UIX$_c$ and NNLO$_{sat}$ predict rather different density surfaces. Roughly similar considerations hold for ^{90}Zr, except that the discrepancy of AV4$'$ + UIX$_c$ with the (2,5,6) EDF, as well as with NNLO$_{sat}$, is more accentuated.

In conclusion, the NNLO$_{sat}$-based LDA EDF compares favorably with the experiment, in spite of its simplicity, and reproduces radii, energies, and densities fairly well in magic nuclei, especially in the heavier ones. The AV4$'$ + UIX$_c$-based EDF, on the other hand, is less satisfactory and highlights even more clearly the necessity of introducing surface terms.

C. Predictions of the GA EDFs

In Sec. III C, simple GA EDFs have been introduced by complementing LDA with two gradient terms and one spin-orbit term. In this section, the predictions of the GA EDFs based on NNLO$_{sat}$ and AV4$'$ + UIX$_c$ are discussed. The parameters C_0^Δ, C_1^Δ, and W_0 are tuned by grid searching over physically reasonable intervals and the results for the four EDFs that yield the smallest rms errors on binding energies or charge radii, called GA-E and GA-r for short, are shown. The corresponding parameters are reported in Table IV. The three parameters are measured in MeV fm^5; from now on, for simplicity the dimension is omitted.

In the case of the NNLO$_{sat}$-based EDF (2,3,4,5,6), we have considered C_0^Δ and C_1^Δ in the intervals $[-40, 0]$ and $[0, 40]$ in steps of 5, while we have varied W_0 between 30 and 140
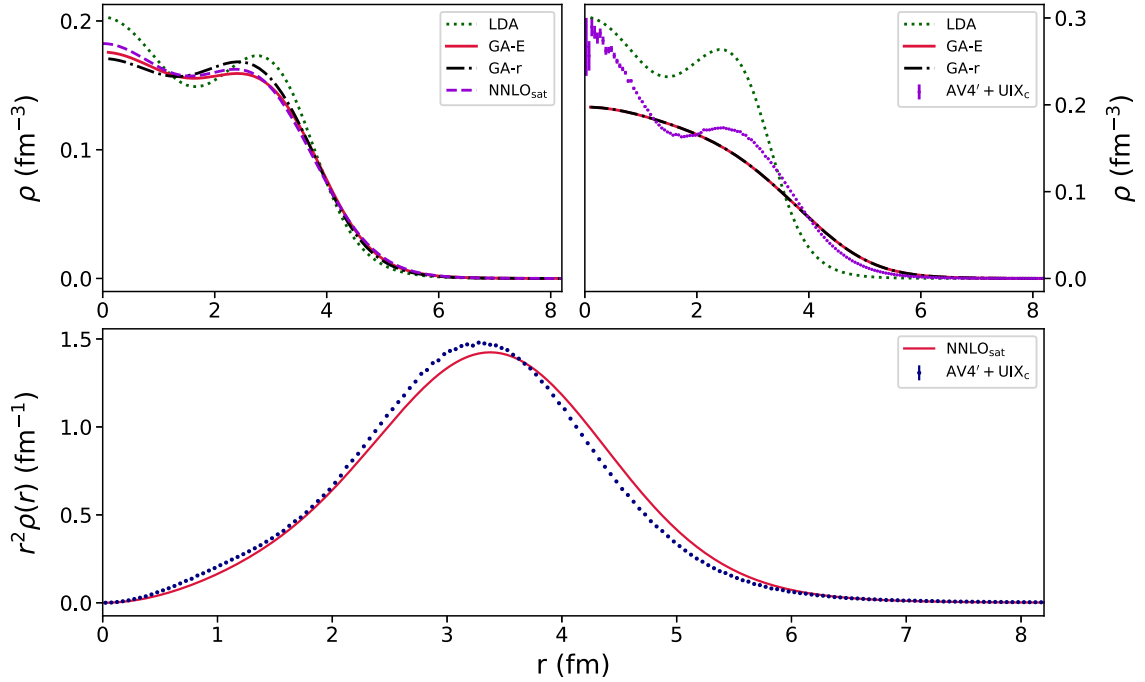
FIG. 5. *Ab initio* and EDF (LDA, GA-E, and GA-r) number densities, $\rho(r)$, for ^{48}Ca computed using the NNLO$_{sat}$ (top left) and AV4$'$ + UIX$_c$ (top right) Hamiltonians. See text for details. Note that for the AV4$'$ + UIX$_c$ case the GA-E and GA-r curves overlap closely. Bottom: *ab initio* number densities times the squared radius, $r^2\rho(r)$, obtained with NNLO$_{sat}$ (full line) and AV4$'$ + UIX$_c$ (dotted).

in steps of 10. The smallest rms error on the energy is obtained for $(C_0^\Delta = -25, C_1^\Delta = 10, W_0 = 50)$, while charge radii are best reproduced for $(C_0^\Delta = -30, C_1^\Delta = 25, W_0 = 140)$

(Table V). The remarkable improvement over the LDA EDF can be appreciated by looking at energies and radii (Fig. 3). In Figs. 5 and 6, the effect of the gradient terms on the number
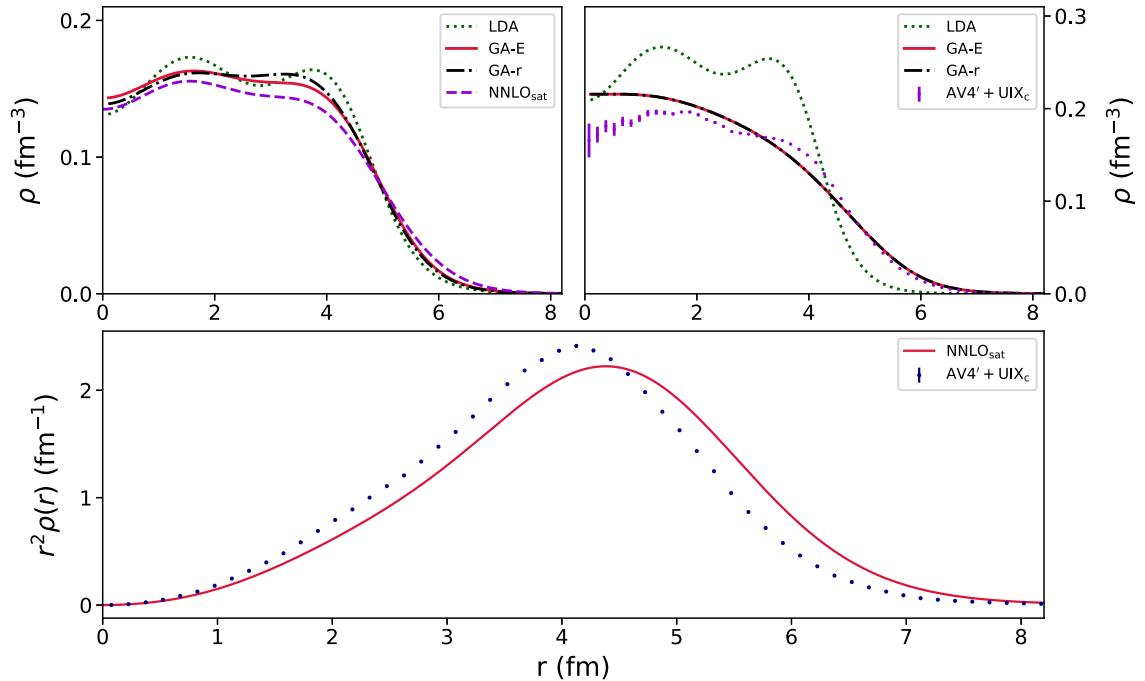

FIG. 6. *Ab initio* and EDF (LDA, GA-E, and GA-r) number densities of ^{90}Zr obtained from NNLO$_{sat}$ (top left) and AV4$'$ + UIX$_c$ (top right). Note that for the AV4$'$ + UIX$_c$ case the GA-E and GA-r curves overlap closely. Bottom: *ab initio* results for $r^2\rho(r)$ using NNLO$_{sat}$ (full line) and AV4$'$ + UIX$_c$ (dotted).

TABLE IV. Coefficients $C_0^{\Delta\rho}$, $C_1^{\Delta\rho}$, and W_0 of the GA-E and GA-r EDFs based on the NNLO$_{sat}$ and AV4$'$ + UIX$_c$ EoS. The GA EDFs are built on top of the LDA EDFs (2,3,4,5,6) in the NNLO$_{sat}$ case and (2,5,6) in the AV4$'$ + UIX$_c$ case (Table III). GA-E and GA-r stand for the GA EDFs that achieve the smallest discrepancy for binding energies and charge radii, respectively. All three parameters are measured in MeV fm^5.

	EDF	$C_0^{\Delta\rho}$	$C_1^{\Delta\rho}$	W_0
NNLO$_{sat}$	GA-E	−25	10	50
	GA-r	−30	25	140
AV4$'$ + UIX$_c$	GA-E	−155	0	10
	GA-r	−155	15	10

densities is made clear by the disappearance of the oscillations which instead characterize the LDA densities. All considered, these GA EDFs are quite accurate, in spite of containing only three adjustable parameters, one of which (C_1^{Δ}) is of minor importance for the g.s. properties. A full-fledged optimization would be necessary at a later stage of development to be truly competitive against the most sophisticated existing EDFs. However, the outcomes shown here are already a very encouraging starting point.

In the case of AV4$'$ + UIX$_c$-based EDFs, C_0^{Δ}, C_1^{Δ}, and W_0 have been varied in the intervals [−200, −60], [0,50], and [0,150]. The smallest errors on radii and energies are obtained with ($C_0^{\Delta} = -155$, $C_1^{\Delta} = 15$, $W_0 = 10$) (GA-r) and ($C_0^{\Delta} = -155$, $C_1^{\Delta} = 0$, $W_0 = 10$) (GA-E), respectively. Highly repulsive gradient contributions are needed to compensate for the LDA overbinding excess. We also note that GA-r and GA-E have quite similar parameters and as a consequence lead to almost indistinguishable outcomes. The GA EDFs perform significantly better than the LDA (2,5,6) EDF (Table V). Surface terms are effective in improving the binding energies, which are brought less than 1 MeV/A from experiment and quite close to AFDMC predictions (top panel of Fig. 4). Note, however, that the scale is different from that of Fig. 3, and that NNLO$_{sat}$-based EDFs are nonetheless more accurate. Some problems persist concerning radii (bottom panel of Fig. 4), which are still inaccurate for the nuclear DFT standards.

TABLE V. Rms errors between theoretical predictions and experimental data on the binding energies per nucleon $\sigma_{E/A}$, total energies σ_E, and charge radii $\sigma_{r_{ch}}$. Calculations are performed with two sets of EDFs, based on the NNLO$_{sat}$ and AV4$'$ + UIX$_c$ EoS. The LDA EDFs are based on the (2,3,4,5,6) EoS in the NNLO$_{sat}$ case and on (2,5,6) EoS in the AV4$'$ + UIX$_c$ case. The rms errors are evaluated on the same set of magic nuclei data as in Ref. [96].

	EDF	$\sigma_{E/A}$ (MeV)	σ_E (MeV)	$\sigma_{r_{ch}}$ (fm)
NNLO$_{sat}$	LDA	1.07	59	0.10
	GA-E	0.30	13	0.03
	GA-r	0.34	21	0.01
AV4$'$ + UIX$_c$	LDA	7.4	800	0.67
	GA-E	0.81	112	0.22
	GA-r	0.77	120	0.21

The different behavior of the NNLO$_{sat}$- and AV4$'$ + UIX$_c$-based EDFs calls for an explanation. The unrealistic saturation density of the AV4$'$ + UIX$_c$ EoS may correlate with LDA predictions being far from experiment. Also, it may explain, at least partially, why radii are not accurate, even at the GA level. However, it cannot explain the large discrepancies of LDA (and GA, as far as radii are concerned) with respect to *ab initio* itself. We then suggest that the strong correlations induced by the hard core of the Argonne interaction may be difficult to catch within LDA, whereas the same scheme can be more successfully applied to the relatively soft NNLO$_{sat}$ potential. The wide oscillations of the AV4$'$ + UIX$_c$ densities may witness the role of short-range correlations. Further investigations should focus on finding a quantitative measure of "hardness" appropriate for this problem [70].

V. CONCLUSION

The present paper outlined a strategy for grounding nuclear DFT into *ab initio* theory, which is systematic in three respects. First, following the "Jacob's ladder" approach of electronic DFT [49], we propose to define a sequence of EDFs with increasing complexity. The starting point is the local density approximation, which allows one to derive the EDFs from the *ab initio* nuclear EoS. Second, different microscopic interactions should be considered as input to the EDF models, in order to assess the sensitivity to this choice and the resulting uncertainty. Third, modern statistical tools should be employed to validate the EDFs and to provide reliable uncertainties on their predictions.

We have thoroughly analyzed the LDA step, using two distinct EoSs, computed with two interactions and many-body methods, i.e., NNLO$_{sat}$ with SCGF and AV4$'$ + UIX$_c$ with AFDMC. A parametrization of the EoS as a polynomial of the Fermi momentum has been proposed and its effectiveness in representing the theoretical curves has been rigorously discussed. The optimal models have been fed as input to the LDA scheme, allowing the construction of simple *ab initio* based EDFs. Moreover, we have introduced a set of elementary GA EDFs, defined by complementing LDA EDFs with phenomenological surface (density-gradient and spin-orbit) terms. Both LDA and GA EDFs have been tested on the g.s. of magic nuclei and compared to *ab initio* and experiment. It must be stressed that we have attempted here only a preliminary GA implementation, while an *ab initio* treatment, fully coherent with the approach described above, will be the subject of future works.

The NNLO$_{sat}$-based EDFs show very interesting results. The simple LDA EDFs only incorporate information on uniform matter but they fairly reproduce charge radii and binding energies. The agreement with the experiment is particularly good for the heaviest nuclei we have tested. Moreover, the predictive power improves considerably at the GA level, although more advanced studies are necessary to compare with the most sophisticated empirical EDFs. In contrast, the AV4$'$ + UIX$_c$ case is somewhat puzzling and the LDA appears to be much less satisfactory in our computations. We observe that very repulsive gradient contributions are needed at the GA level and do make an important effect, significantly shrinking the

discrepancy with AFDMC calculations. Still, some more issues persist; in particular, radii compare to experiment in an unsatisfactory way for the DFT standards.

The different behavior of NNLO$_\text{sat}$- and AV4′ + UIX$_c$-based EDFs needs to be understood. We suggest that LDA may struggle to catch the strong correlations induced by the hard core of the Argonne interaction, while NNLO$_\text{sat}$, that is a relatively soft potential, may be more amenable to this approximate mapping onto LDA. Further investigations of this hypothesis will require seeking an appropriate quantitative measure of the hardness of these interactions [70]. Energy densities, although they are not observables, may be useful to link *ab initio* and DFT [100]. For example, they may help clarifying to what extent *ab initio* calculations meet the hypothesis that underlie LDA.

We find that the quality of predictions obtained in the present exploratory paper is promising, in particular for the NNLO$_\text{sat}$ interaction. Therefore, we will aim at extending our paper in several directions. First of all, future studies will focus on constraining the gradient terms systematically on *ab initio*, with the help of simulations of model systems, such as neutron/proton drops [101] or the static or dynamic response of nuclear matter [9,102,103].

Also, some of the surface terms of empirical EDFs give rise to the so-called effective mass, which is known to be crucial to the description of the nuclear spectroscopy. A second parallel line of development will aim at exploiting more refined statistical tools. As mentioned, Bayesian statistics [56,57] or machine learning techniques [54] can play a determinant role in the calibration and assessment of the EDFs. Providing error bars on the EDF predictions would be a very important step forward. Lastly, we plan to apply these EDFs on a wider range of physical problems, including time-dependent DFT.

APPENDIX A: LDA MEAN FIELD POTENTIAL

We derive the mean field potential $U_q(\mathbf{r})$ for the LDA EDF in Sec. III C. By definition,

$$U_q(\mathbf{r}) = \frac{\delta E_\text{bulk}}{\delta \rho_q(\mathbf{r})} = \frac{\partial \mathcal{E}_\text{bulk}}{\partial \rho_q} = \frac{\partial \mathcal{E}_\text{bulk}}{\partial \rho} + \frac{\partial \beta}{\partial \rho_q}\frac{\partial \mathcal{E}_\text{bulk}}{\partial \beta} \quad \text{(A1)}$$

with $q = n, p$. Using $\rho = \rho_n + \rho_p$ and $\beta = \frac{\rho_n - \rho_p}{\rho}$, the chain rule leads to the following contributions:

$$\frac{\partial \beta}{\partial \rho_q} = \frac{1}{\rho}\frac{\partial}{\partial \rho_q}(\rho_n - \rho_p) + \quad \text{(A2)}$$

$$(\rho_n - \rho_p)\left(-\frac{1}{\rho^2}\right)\frac{\partial \rho}{\partial \rho_q} = \frac{\tau_z - \beta}{\rho},$$

$$\frac{\partial \mathcal{E}_\text{loc}}{\partial \rho} = \sum_\gamma (\gamma + 1)c_\gamma(\beta)\rho^\gamma, \quad \text{(A3)}$$

$$\frac{\partial \mathcal{E}_\text{loc}}{\partial \beta} = \sum_\gamma \frac{\partial c_\gamma(\beta)}{\partial \beta}\rho^\gamma = 2\beta\sum_\gamma c_{\gamma,1}\rho^{\gamma+1} \quad \text{(A4)}$$

where $\tau_z = +1$ for neutrons and $\tau_z = -1$ for protons. Therefore

$$U_q = \sum_\gamma (\gamma + 1)c_\gamma(\beta)\rho^\gamma + (\tau_z - \beta)2\beta\sum_\gamma c_{\gamma,1}\rho^\gamma$$

$$= \sum_\gamma [(\gamma + 1)c_\gamma(\beta)\rho^\gamma + 2\beta(\tau_z - \beta)c_{\gamma,1}]\rho^\gamma$$

and finally

$$U_q(\mathbf{r}) = \sum_\gamma [(\gamma + 1)c_{\gamma,0} + 2\beta(\tau_z - \beta)c_{\gamma,1}$$

$$+ (\gamma + 1)c_{\gamma,1}\beta^2]\rho^\gamma,$$

which proves Eq. (27).

APPENDIX B: GA MEAN FIELD POTENTIAL

The mean field U_q^surf Eq. (31) is derived. By definition, $U_q^\text{surf}(\mathbf{r}) = \frac{\delta E_\text{surf}}{\delta \rho_q}$, where E_surf is conveniently written as the volume integral of the density:

$$\mathcal{E}_\text{surf} = -\sum_{t=0,1} C_t^\Delta |\nabla \rho_t|^2$$

$$- \frac{W_0}{2}(\rho \nabla \cdot \mathbf{J} + \rho_n \nabla \cdot \mathbf{J}_n + \rho_p \nabla \cdot \mathbf{J}_p).$$

Then

$$\frac{\delta E_\text{surf}}{\delta \rho_q}(r) = \frac{\partial \mathcal{E}_\text{surf}}{\partial \rho_q} - \nabla \cdot \left(\frac{\partial \mathcal{E}_\text{surf}}{\partial (\nabla \rho_q)}\right). \quad \text{(B1)}$$

The first contribution is due to the spin-orbit part and is equal to

$$\frac{\partial \mathcal{E}_\text{surf}}{\partial \rho_q} = -\frac{W_0}{2}(\nabla \cdot \mathbf{J} + \nabla \cdot \mathbf{J}_q). \quad \text{(B2)}$$

The second one is due to the gradient terms of the EDF. To compute it, we first insert $\rho_0 = \rho_n + \rho_p$ and $\rho_1 = \rho_n - \rho_p$ into the energy density,

$$\mathcal{E}_\text{surf} = -(C_0^\Delta + C_1^\Delta)(|\nabla \rho_n|^2 + |\nabla \rho_p|^2)$$

$$+ 2(C_1^\Delta - C_0^\Delta)\nabla \rho_n \cdot \nabla \rho_p,$$

and then take the derivative:

$$-\nabla \cdot \left(\frac{\partial \mathcal{E}_{\text{surf}}}{\partial (\nabla \rho_q)} \right)$$

$$= 2(C_0^\Delta + C_1^\Delta)\Delta\rho_q - 2(C_1^\Delta - C_0^\Delta)\Delta\rho_{\bar{q}}$$

$$= 2C_0^\Delta(\Delta\rho_q + \Delta\rho_{\bar{q}}) + 2C_1^\Delta(\Delta\rho_q - \Delta\rho_{\bar{q}})$$

$$= 2C_0^\Delta \Delta\rho_0 + 2C_1^\Delta \Delta\rho_1 \tau_z \qquad \text{(B3)}$$

where $\bar{q} = p$ if $q = n$ and vice versa. Summing Eqs. (B2) and (B3) concludes the derivation.

APPENDIX C: REARRANGEMENT ENERGY

In nuclear DFT, the total energy can be computed in two independent ways: (1) as the space integral of the EDF evaluated on the ground-state densities that one obtains by solving the mean field equations,

$$E = \int d\mathbf{r}\, \mathcal{E}(\mathbf{r}), \qquad \text{(C1)}$$

and (2) with the Hartree-Fock (HF) formula for a density-dependent Hamiltonian [87]:

$$E = \frac{1}{2}\left(T + \sum_k \epsilon_k \right) + E_{\text{rea}}. \qquad \text{(C2)}$$

The extra term E_{rea} is called rearrangement energy. The equality of the two expressions for the binding energy is often used as a nontrivial test of the correctness of the implementation of a DFT or HF code.

Here, the rearrangement energy for the LDA EDF of Sec. III C is derived. The following practical definition is employed:

$$E_{\text{rea}} = \int d\mathbf{r}\, \mathcal{E}_{\text{bulk}}(\mathbf{r}) - \frac{1}{2}\sum_q \int d\mathbf{r} U_q(\mathbf{r})\rho_q(\mathbf{r}) \qquad \text{(C3)}$$

with the mean field $U_q(\mathbf{r})$ (27). Then

$$\sum_q U_q\rho_q = U_n\rho_n + U_p\rho_p$$

$$= [U_n(1+\beta) + U_p(1-\beta)]\frac{\rho}{2}$$

$$= [(U_n + U_p) + (U_n - U_p)\beta]\frac{\rho}{2}.$$

We calculate $U_n + U_p$ and $U_n - U_p$ separately:

$$U_n + U_p = 2\sum_\gamma [(\gamma+1)c_{\gamma,0} - 2\beta^2 c_{\gamma,1} + (\gamma+1)\beta^2 c_{\gamma,1}]\rho^\gamma$$

$$= 2\sum_\gamma [(\gamma+1)c_{\gamma,0} + (\gamma-1)\beta^2 c_{\gamma,1}]\rho^\gamma$$

and

$$U_n - U_p = 4\beta \sum_\gamma c_{\gamma,1}\rho^\gamma$$

with $\tau_z = 1$ for neutrons and $\tau_z = -1$ for protons. Then

$$\sum_q U_q\rho_q = \frac{\rho}{2} 2\sum_\gamma [(\gamma+1)c_{\gamma,0} + (\gamma+1)\beta^2 c_{\gamma,1}]\rho^{\gamma+1}.$$

Plugging into the definitions of E_{rea}

$$E_{\text{rea}} = \int d\mathbf{r} \sum_\gamma \left[(c_{\gamma,0} + \beta^2 c_{\gamma,1})\rho^{\gamma+1} \right.$$

$$\left. - \left(\frac{1+\gamma}{2} \right)(c_{\gamma,0} + \beta^2 c_{\gamma,1})\rho^{\gamma+1} \right]$$

and finally

$$E_{\text{rea}} = \int d\mathbf{r} \sum_\gamma \left(\frac{1-\gamma}{2} \right)(c_{\gamma,0} + \beta^2 c_{\gamma,1})\rho^{\gamma+1}. \qquad \text{(C4)}$$

[1] W. Leidemann and G. Orlandini, Prog. Part. Nucl. Phys. **68**, 158 (2013).

[2] M. Hjorth-Jensen, M.-P. Lombardo, and U. van Kolck, An advanced course in computational nuclear physics: Bridging the scales from quarks to neutron stars, in *An Advanced Course in Computational Nuclear Physics*, Lecture Notes in Physics, Vol. 936 (Springer International Publishing AG, Cham, 2017).

[3] H. Hergert, Front. Phys. **8**, 00379 (2020).

[4] J. Carlson, S. Gandolfi, F. Pederiva, S. C. Pieper, R. Schiavilla, K. E. Schmidt, and R. B. Wiringa, Rev. Mod. Phys. **87**, 1067 (2015).

[5] J. Lynn, I. Tews, S. Gandolfi, and A. Lovato, Annu. Rev. Nucl. Part. Sci. **69**, 279 (2019).

[6] S. Gandolfi, D. Lonardoni, A. Lovato, and M. Piarulli, Front. Phys. **8**, 00117 (2020).

[7] W. Dickhoff and C. Barbieri, Prog. Part. Nucl. Phys. **52**, 377 (2004).

[8] C. Barbieri and A. Carbone, Self-consistent Green's function approaches, in *An Advanced Course in Computational Nuclear Physics: Bridging the Scales from Quarks to Neutron Stars*, edited by M. Hjorth-Jensen, M. P. Lombardo, and U. van Kolck (Springer, New York, 2017), pp. 571–644.

[9] A. Rios, Front. Phys. **8**, 387 (2020).

[10] V. Somà, Front. Phys. **8**, 340 (2020).

[11] G. Hagen, T. Papenbrock, M. Hjorth-Jensen, and D. J. Dean, Rep. Prog. Phys. **77**, 096302 (2014).

[12] G. Hagen, T. Papenbrock, A. Ekström, K. A. Wendt, G. Baardsen, S. Gandolfi, M. Hjorth-Jensen, and C. J. Horowitz, Phys. Rev. C **89**, 014319 (2014).

[13] H. Hergert, S. Bogner, T. Morris, A. Schwenk, and K. Tsukiyama, Phys. Rep. **621**, 165 (2016).

[14] C. Drischler, K. Hebeler, and A. Schwenk, Phys. Rev. Lett. **122**, 042501 (2019).

[15] A. Tichai, R. Roth, and T. Duguet, Front. Phys. **8**, 164 (2020).

[16] V. Somà, P. Navratil, F. Raimondi, C. Barbieri, and T. Duguet, Phys. Rev. C **101**, 014318 (2020).

[17] D. Lonardoni, I. Tews, S. Gandolfi, and J. Carlson, Phys. Rev. Research **2**, 022033(R) (2020).

[18] A. Carbone, Phys. Rev. Research **2**, 023227 (2020).

[19] F. J. Llanes-Estrada and E. Lope-Oter, Prog. Part. Nucl. Phys. **109**, 103715 (2019).

[20] S. Gandolfi, A. Gezerlis, and J. Carlson, Annu. Rev. Nucl. Part. Sci. **65**, 303 (2015).

[21] P. Arthuis, C. Barbieri, M. Vorabbi, and P. Finelli, Phys. Rev. Lett. **125**, 182501 (2020).

[22] R. G. Parr and W. Yang, *Density-Functional Theory of Atoms and Molecules*, International Series of Monographs on Chemistry (Oxford University, New York, 1994).

[23] R. M. Martin, *Electronic Structure: Basic Theory and Practical Methods* (Cambridge University, Cambridge, England, 2004).

[24] A. D. Becke, J. Chem. Phys. **140**, 18A301 (2014).

[25] K. Burke, J. Chem. Phys. **136**, 150901 (2012).

[26] G. Colò, Adv. Phys.-X **5**, 1740061 (2020).

[27] *Energy Density Functional Methods for Atomic Nuclei*, edited by N. Schunck (IOP Publishing, 2019).

[28] M. Bender, P.-H. Heenen, and P.-G. Reinhard, Rev. Mod. Phys. **75**, 121 (2003).

[29] T. Nakatsukasa, K. Matsuyanagi, M. Matsuo, and K. Yabana, Rev. Mod. Phys. **88**, 045004 (2016).

[30] J. Dobaczewski, J. Phys.: Conf. Ser. **312**, 092002 (2011).

[31] J. Stone and P.-G. Reinhard, Prog. Part. Nucl. Phys. **58**, 587 (2007).

[32] P. Hohenberg and W. Kohn, Phys. Rev. **136**, B864 (1964).

[33] P. Chomaz and K. Hasnaoui, arXiv:nucl-th/0610027v2.

[34] D. Vretenar, A. Afanasjev, G. Lalazissis, and P. Ring, Phys. Rep. **409**, 101 (2005).

[35] E. Chabanat, P. Bonche, P. Haensel, J. Meyer, and R. Schaeffer, Nucl. Phys. A **627**, 710 (1997).

[36] M. Kortelainen, J. McDonnell, W. Nazarewicz, E. Olsen, P.-G. Reinhard, J. Sarich, N. Schunck, S. M. Wild, D. Davesne, J. Erler, and A. Pastore, Phys. Rev. C **89**, 054314 (2014).

[37] R. J. Furnstahl, European Phys. J. A **56**, 85 (2020).

[38] M. Grasso, Prog. Part. Nucl. Phys. **106**, 256 (2019).

[39] J. Dobaczewski, J. Phys. G: Nucl. Part. Phys. **43**, 04LT01 (2016).

[40] G. Salvioni, J. Dobaczewski, C. Barbieri, G. Carlsson, A. Idini, and A. Pastore, J. Phys. G **47**, 085107 (2020).

[41] R. Navarro Pérez, N. Schunck, A. Dyhdalo, R. J. Furnstahl, and S. K. Bogner, Phys. Rev. C **97**, 054304 (2018).

[42] L. Zurek, E. A. Coello Pérez, S. K. Bogner, R. J. Furnstahl, and A. Schwenk, Phys. Rev. C **103**, 014325 (2021).

[43] M. Baldo, P. Schuck, and X. Viñas, Phys. Lett. B **663**, 390 (2008).

[44] M. Baldo, L. M. Robledo, P. Schuck, and X. Viñas, Phys. Rev. C **87**, 064305 (2013).

[45] X. Roca-Maza, X. Viñas, M. Centelles, P. Ring, and P. Schuck, Phys. Rev. C **84**, 054309 (2011).

[46] D. Gambacurta, L. Li, G. Colò, U. Lombardo, N. Van Giai, and W. Zuo, Phys. Rev. C **84**, 024301 (2011).

[47] P. Papakonstantinou, T.-S. Park, Y. Lim, and C. H. Hyun, Phys. Rev. C **97**, 014312 (2018).

[48] A. Bulgac, M. M. Forbes, S. Jin, R. N. Perez, and N. Schunck, Phys. Rev. C **97**, 044313 (2018).

[49] J. P. Perdew and K. Schmidt, AIP Conf. Proc. **577**, 1 (2001).

[50] M. G. Medvedev, I. S. Bushmarinov, J. Sun, J. P. Perdew, and K. A. Lyssenko, Science **355**, 49 (2017).

[51] J. P. Perdew, K. Burke, and M. Ernzerhof, Phys. Rev. Lett. **77**, 3865 (1996).

[52] R. Machleidt and F. Sammarruca, Eur. Phys. J. A **56**, 95 (2020).

[53] D. M. Ceperley and B. J. Alder, Phys. Rev. Lett. **45**, 566 (1980).

[54] P. Mehta, M. Bukov, C.-H. Wang, A. G. Day, C. Richardson, C. K. Fisher, and D. J. Schwab, Phys. Rep. **810**, 1 (2019).

[55] T. Hastie, R. Tibshirani, and J. Friedman, *The Elements of Statistical Learning: Data Mining, Inference and Prediction*, 2nd ed. (Springer, New York, 2009).

[56] U. von Toussaint, Rev. Mod. Phys. **83**, 943 (2011).

[57] C. Drischler, J. A. Melendez, R. J. Furnstahl, and D. R. Phillips, Phys. Rev. C **102**, 054315 (2020).

[58] D. Lonardoni and F. Pederiva, arXiv:1711.07521.

[59] R. B. Wiringa and S. C. Pieper, Phys. Rev. Lett. **89**, 182501 (2002).

[60] R. B. Wiringa, V. G. J. Stoks, and R. Schiavilla, Phys. Rev. C **51**, 38 (1995).

[61] A. Ekström, G. R. Jansen, K. A. Wendt, G. Hagen, T. Papenbrock, B. D. Carlsson, C. Forssén, M. Hjorth-Jensen, P. Navrátil, and W. Nazarewicz, Phys. Rev. C **91**, 051301(R) (2015).

[62] E. Epelbaum, H.-W. Hammer, and Ulf-G. Meißner, Rev. Mod. Phys. **81**, 1773 (2009).

[63] R. Machleidt and F. Sammarruca, Phys. Scr. **91**, 083007 (2016).

[64] E. Epelbaum, H. Krebs, and P. Reinert, Front. Phys. **8**, 98 (2020).

[65] A. Gezerlis, I. Tews, E. Epelbaum, S. Gandolfi, K. Hebeler, A. Nogga, and A. Schwenk, Phys. Rev. Lett. **111**, 032501 (2013).

[66] J. E. Lynn, J. Carlson, E. Epelbaum, S. Gandolfi, A. Gezerlis, and A. Schwenk, Phys. Rev. Lett. **113**, 192501 (2014).

[67] M. Piarulli, L. Girlanda, R. Schiavilla, A. Kievsky, A. Lovato, L. E. Marcucci, S. C. Pieper, M. Viviani, and R. B. Wiringa, Phys. Rev. C **94**, 054007 (2016).

[68] M. Piarulli, A. Baroni, L. Girlanda, A. Kievsky, A. Lovato, E. Lusk, L. E. Marcucci, S. C. Pieper, R. Schiavilla, M. Viviani, and R. B. Wiringa, Phys. Rev. Lett. **120**, 052503 (2018).

[69] D. Lonardoni, S. Gandolfi, J. E. Lynn, C. Petrie, J. Carlson, K. E. Schmidt, and A. Schwenk, Phys. Rev. C **97**, 044318 (2018).

[70] A. Rios, A. Carbone, and A. Polls, Phys. Rev. C **96**, 014003 (2017).

[71] T. Hüther, K. Vobig, K. Hebeler, R. Machleidt, and R. Roth, Phys. Lett. B **808**, 135651 (2020).

[72] F. Sammarruca and R. Millerson, Phys. Rev. C **102**, 034313 (2020).

[73] D. Lonardoni, arXiv:1311.6672.

[74] V. Somà, C. Barbieri, and T. Duguet, Phys. Rev. C **87**, 011303(R) (2013).

[75] A. Carbone, A. Rios, and A. Polls, Phys. Rev. C **90**, 054322 (2014).

[76] A. Carbone, A. Cipollone, C. Barbieri, A. Rios, and A. Polls, Phys. Rev. C **88**, 054326 (2013).

[77] A. Rios, A. Polls, and I. Vidaña, Phys. Rev. C **79**, 025802 (2009).

[78] W. M. C. Foulkes, L. Mitas, R. J. Needs, and G. Rajagopal, Rev. Mod. Phys. **73**, 33 (2001).

[79] K. E. Schmidt and S. Fantoni, Phys. Lett. B **446**, 99 (1999).

[80] J. E. Lynn, I. Tews, J. Carlson, S. Gandolfi, A. Gezerlis, K. E. Schmidt, and A. Schwenk, Phys. Rev. Lett. **116**, 062501 (2016).

[81] L. Contessi, A. Lovato, F. Pederiva, A. Roggero, J. Kirscher, and U. van Kolck, Phys. Lett. B **772**, 839 (2017).

[82] R. Schiavilla, L. Girlanda, A. Gnech, A. Kievsky, A. Lovato, L. E. Marcucci, M. Piarulli, and M. Viviani, Phys. Rev. C **103**, 054003 (2021).

[83] A. Sarsa, S. Fantoni, K. E. Schmidt, and F. Pederiva, Phys. Rev. C **68**, 024308 (2003).

[84] B. R. Barrett, P. Navratil, and J. P. Vary, Prog. Part. Nucl. Phys. **69**, 131 (2013).

[85] E. D. Jurgenson, P. Maris, R. J. Furnstahl, P. Navratil, W. E. Ormand, and J. P. Vary, Phys. Rev. C **87**, 054312 (2013).

[86] M. Piarulli, I. Bombaci, D. Logoteta, A. Lovato, and R. B. Wiringa, Phys. Rev. C **101**, 045801 (2020).

[87] P. Ring and P. Schuck, *The Nuclear Many-Body Problem* (Springer, New York, 1980).

[88] G. Colò, L. Cao, N. V. Giai, and L. Capelli, Comput. Phys. Commun. **184**, 142 (2013).

[89] J. Margueron, R. Hoffmann Casali, and F. Gulminelli, Phys. Rev. C **97**, 025805 (2018).

[90] X. Roca-Maza and N. Paar, Prog. Part. Nucl. Phys. **101**, 96 (2018).

[91] I. Tews, Front. Phys. **8**, 153 (2020).

[92] U. Garg and G. Coló, Prog. Part. Nucl. Phys. **101**, 55 (2018).

[93] N. Kaiser, S. Fritsch, and W. Weise, Nucl. Phys. A **697**, 255 (2002).

[94] R. Andrae, T. Schulze-Hartung, and P. Melchior, arXiv:1012.3754.

[95] F. Pedregosa, G. Varoquaux, A. Gramfort, V. Michel, B. Thirion, O. Grisel, M. Blondel, P. Prettenhofer, R. Weiss, V. Dubourg, J. Vanderplas, A. Passos, D. Cournapeau, M. Brucher, M. Perrot, and E. Duchesnay, Journal of Machine Learning Research **12**, 2825 (2011).

[96] X. Roca-Maza, G. Colò, and H. Sagawa, Phys. Rev. C **86**, 031306(R) (2012).

[97] M. Baldo, A. Polls, A. Rios, H.-J. Schulze, and I. Vidaña, Phys. Rev. C **86**, 064001 (2012).

[98] I. Angeli and K. Marinova, At. Data Nucl. Data Tables **99**, 69 (2013).

[99] M. Wang, G. Audi, F. G. Kondev, W. Huang, S. Naimi, and X. Xu, Chin. Phys. C **41**, 030003 (2017).

[100] M. C. Atkinson, W. H. Dickhoff, M. Piarulli, A. Rios, and R. B. Wiringa, Phys. Rev. C **102**, 044333 (2020).

[101] S. Gandolfi, J. Carlson, and S. C. Pieper, Phys. Rev. Lett. **106**, 012501 (2011).

[102] M. Buraczynski and A. Gezerlis, Phys. Rev. C **95**, 044309 (2017).

[103] M. Buraczynski, S. Martinello, and A. Gezerlis, Phys. Lett. B **818**, 136347 (2021).